



HAL
open science

Investigation of the convergence of the mixed displacement-pressure formulation for three-dimensional poroelastic materials using hierarchical elements

Stéphane Rigobert, Nouredine Atalla, Franck Sgard

► **To cite this version:**

Stéphane Rigobert, Nouredine Atalla, Franck Sgard. Investigation of the convergence of the mixed displacement-pressure formulation for three-dimensional poroelastic materials using hierarchical elements. *Journal of the Acoustical Society of America*, 2003, 114 (5), pp.2607. 10.1121/1.1616579 . hal-03688794

HAL Id: hal-03688794

<https://hal.science/hal-03688794>

Submitted on 6 Jun 2022

HAL is a multi-disciplinary open access archive for the deposit and dissemination of scientific research documents, whether they are published or not. The documents may come from teaching and research institutions in France or abroad, or from public or private research centers.

L'archive ouverte pluridisciplinaire **HAL**, est destinée au dépôt et à la diffusion de documents scientifiques de niveau recherche, publiés ou non, émanant des établissements d'enseignement et de recherche français ou étrangers, des laboratoires publics ou privés.



Distributed under a Creative Commons Attribution - NonCommercial 4.0 International License

Investigation of the convergence of the mixed displacement-pressure formulation for three-dimensional poroelastic materials using hierarchical elements

S. Rigobert

Laboratoire des Sciences de l'Habitat, DGCB URA CNRS 1652, Ecole Nationale des Travaux Publics de l'Etat, 69518 Vaulx-en-Velin Cedex, France

N. Atalla

Groupe d'Acoustique de l'Université de Sherbrooke, Department of Mechanical Engineering, University of Sherbrooke, Sherbrooke, Quebec J1K 2R1, Canada

F. C. Sgard

Laboratoire des Sciences de l'Habitat, DGCB URA CNRS 1652, Ecole Nationale des Travaux Publics de l'Etat, 69518 Vaulx-en-Velin Cedex, France

Recently, a mixed pressure displacement $\{\mathbf{u}, \mathbf{P}\}$ formulation based on Biot's poroelasticity equations has been presented for porous materials. This model leads to a reduction of the number of degrees of freedom required for the modeling of three-dimensional porous media in comparison to classical displacement-displacement $\{\mathbf{u}, \mathbf{U}\}$ formulations. In this paper, an extension of the $\{\mathbf{u}, \mathbf{P}\}$ formulation based on hierarchical elements is presented. First, a variant of the weak integral form of the $\{\mathbf{u}, \mathbf{P}\}$ formulation is presented and its numerical implementation using hierarchical elements is detailed, together with the application of boundary and loading conditions. Numerical results are presented to show the accuracy and performance of the present approach. In particular, the importance of correctly capturing the coupling effects between the two phases is highlighted.

I. INTRODUCTION

The behavior of porous material is classically modeled using empirical formulas for locally reacting materials,¹ or with accurate one-dimensional (1D) analytical methods based on Biot poroelasticity theory.²⁻⁵ At low frequencies, where the modal behavior of the system is important, several two-dimensional (2D) and three-dimensional (3D) finite elements models have been developed. The first models use, with different variations, the displacement fields in the solid and fluid phase of the porous material as variables.⁶⁻¹⁰ They are referred to as $\{\mathbf{u}, \mathbf{U}\}$ type formulations. While accurate, the $\{\mathbf{u}, \mathbf{U}\}$ formulations lead to large frequency dependent systems and thus to cumbersome calculations for complex structures. To alleviate the problem, Atalla *et al.*¹¹ presented an exact mixed displacement-pressure $\{\mathbf{u}, \mathbf{P}\}$ finite element formulation in three dimensions for a porous material, based on Biot's poroelastic equations. Debergue *et al.*¹² presented the boundary and coupling conditions for this new formulation. Atalla *et al.*' model presents the calculation of the response of the porous material in the form of a coupled fluid-structure problem. This formulation has been proven to give accurate results when compared to the $\{\mathbf{u}, \mathbf{U}\}$ formulation. More importantly, by reducing the number of degrees of freedom involved (i.e., from six degrees of freedom per node to four) and by simplifying the coupling conditions between the porous medium and elastic or fluid media, the approach leads to important gains in memory and computation time requirements.

While the $\{\mathbf{u}, \mathbf{P}\}$ formulation allows for a more efficient

modeling to porous elastic media compared to the $\{\mathbf{u}, \mathbf{U}\}$ formulation, yet both techniques suffer from important computational costs in practical applications. Indeed, because of the biphasic nature of poroelastic elements, mesh criterion used for elements describing monophasic media (solid, fluid) is *a priori* not valid for poroelastic elements. Using the $\{\mathbf{u}, \mathbf{U}\}$ formulation, Dauchez *et al.*¹³ showed that linear poroelastic elements verify convergence rate of linear monophasic elements, according to each type of Biot wave. Classical mesh criterion, i.e., six linear elements per wavelength, provides a necessary condition to get reliable results. However, for real 3D deformations, the classical criterion gives indications for a minimal mesh but is insufficient because of locking of 3D linear elements and discrepancies in the wavelengths of the displacement fields of the two phases. An important refinement of the mesh is necessary to get satisfactory results. In particular, indicators related to fluid motion have been found very sensitive. As a consequence, the minimal number of elements required is difficult to predict. By nature, convergence of poroelastic elements is rather slower than convergence of either equivalent solid or fluid elements, because of the presence of two different scale phenomena. The discrepancy can be lowered when the behavior of the porous material is dominated by the motion of one phase. As a consequence, this slow convergence leads to large computational costs. Debergue¹⁴ found similar results using the $\{\mathbf{u}, \mathbf{P}\}$ formulation. Several recent attempts to alleviate the computing cost of the poroelastic formulations, using linear elements, have been unsuccessful. For example,

Sgard *et al.*^{15,16} have investigated the use of a selective modal analysis to decrease the size of large finite elements models involving poroelastic materials. The method used a dual uncoupled basis of undamped modes associated with the skeleton *in vacuo* and the fluid phase occupying the volume of the porous material to approximate the $\{\mathbf{u}, \mathbf{P}\}$ variables. However, this method converges poorly due to the importance of the damping brought in by the porous material. The same authors also proposed a mixed wave-finite element approach dedicated to the modeling of porous materials.¹⁷ Starting from the weak $\{\mathbf{u}, \mathbf{P}\}$ formulation for a porous material, the fields for each phase of the porous material were expanded at each node of the finite element mesh in terms of a finite number of wave functions. These functions are chosen to be plane waves solution of Biot's poroelasticity equations. This approach gives accurate results for a single porous material and leads to a considerable reduction of the size of the system to be solved. However, this system is no longer sparse and its construction is time consuming. Another way to solve the computing cost problem, would be to design specific models dedicated to particular applications. For example, Dauchez *et al.*¹⁸ pointed out that most of the extra-energy dissipation related to the foam coating of a plate was due to structural damping in the solid phase of the porous medium. Thus, the porous material could be reduced to its solid phase in such a configuration. However, this assumption can not be generalized, especially for a coating by a glasswool where viscous effects become quickly predominant as frequency increases.¹⁹

In order to solve the convergence problem, it is proposed in this paper to investigate the performance of the $\{\mathbf{u}, \mathbf{P}\}$ formulation using high-order hierarchical elements. It is known that these elements allow for higher order polynomial representation and thus eliminate problems such as locking.^{20–24} Because of the higher order of approximation of hierarchical elements, a more accurate representation of the different type of deformations and coarser meshes, compared to classical finite elements, can be used. Therefore, a significant reduction of the number of degrees of freedom required for a correct modeling is expected. In the first part of the paper, a variant of the $\{\mathbf{u}, \mathbf{P}\}$ formulation is recalled and the theory of hierarchical elements in this context is introduced. In particular, the treatment of the boundary conditions and excitations is detailed. Validation results are then presented to show the accuracy of the present approach. The performance of the hierarchical poroelastic formulation in terms of the needed number of degrees of freedom is underlined, and can be increased by the choice of different interpolation orders for the basis functions in the solid and fluid phase. The interest of this latter feature is shown and guidelines for the convergence of hierarchical poroelastic elements are presented from the study of a particular material.

II. THEORY

This section concentrates on the forced response of a single isotropic porous material. Biot–Allard equations of poroelasticity are considered for the description of the porous medium. The displacement of the solid phase and the interstitial pressure are chosen as variables.

A. The mixed displacement-pressure formulation

The starting point of the modeling of the porous medium is the weak $\{\mathbf{u}, \mathbf{P}\}$ formulation (Atalla *et al.*).¹¹ The mixed displacement-pressure formulation for a poroelastic material occupying a volume Ω_p reads

$$\begin{aligned} & \int_{\Omega_p} [\tilde{\boldsymbol{\sigma}}^S(\mathbf{u}) : \boldsymbol{\varepsilon}^S(\delta\mathbf{u}) - \tilde{\rho}\omega^2\mathbf{u} \cdot \delta\mathbf{u}] d\Omega \\ & + \int_{\Omega_p} \left[\frac{h^2}{\omega^2\tilde{\rho}_{22}} \nabla P \cdot \nabla \delta P - \frac{h^2}{\tilde{R}} P \delta P \right] d\Omega \\ & - \tilde{\gamma} \int_{\Omega_p} \delta(\nabla P \cdot \mathbf{u}) d\Omega - \int_{\partial\Omega_p} h \left(1 + \frac{\tilde{Q}}{\tilde{R}} \right) \\ & \times \delta(Pu_n) dS - \int_{\partial\Omega_p} [\tilde{\boldsymbol{\sigma}}^t(\mathbf{u}) \cdot \mathbf{n}] \cdot \delta\mathbf{u} dS \\ & - \int_{\partial\Omega_p} h(U_n - u_n) \delta P = 0, \end{aligned} \quad (1)$$

where $\partial\Omega_p$ stands for the boundary of the poroelastic domain. \mathbf{u} is the solid phase displacement, \mathbf{U} and P are the displacement and the pressure of the fluid in the pores, respectively. $\tilde{\boldsymbol{\sigma}}^S$ and $\boldsymbol{\varepsilon}^S$ are, respectively, the stress and strain tensor of the solid phase *in vacuo*. The total stress tensor in the porous material $\tilde{\boldsymbol{\sigma}}^t$ is related to $\tilde{\boldsymbol{\sigma}}^S$ by the relation $\tilde{\boldsymbol{\sigma}}^t = \tilde{\boldsymbol{\sigma}}^S - h[1 + (\tilde{Q}/\tilde{R})]P\mathbf{1}$. $\tilde{\rho}$ and $\tilde{\rho}_{22}$ are the apparent density of the solid and the fluid phase, h is the porosity, $\tilde{\gamma}$ is a coupling factor between the two phases, \tilde{Q} and \tilde{R} are poroelastic coefficients. The expressions of the latter quantities can be found in Ref. 11.

Instead of using directly Eq. (1), a variant is presented here. The first surface integral in Eq. (1) can be turned into a volume integral using the second Green formula and given the following mathematical relation:

$$\nabla \cdot (a\mathbf{b}) = \nabla a \cdot \mathbf{b} + a \nabla \cdot (\mathbf{b}). \quad (2)$$

Hence, assuming that the porous material is isotropic,

$$\begin{aligned} I &= - \int_{\partial\Omega_p} h \left(1 + \frac{\tilde{Q}}{\tilde{R}} \right) \delta(u_n P) dS \\ &= - \int_{\Omega_p} \nabla \cdot \left(h \left(1 + \frac{\tilde{Q}}{\tilde{R}} \right) \delta(u_n P) \right) d\Omega \\ &= - h \left(1 + \frac{\tilde{Q}}{\tilde{R}} \right) \int_{\Omega_p} \delta(\mathbf{u} \cdot \nabla P) d\Omega \\ &\quad - h \left(1 + \frac{\tilde{Q}}{\tilde{R}} \right) \int_{\Omega_p} \delta(P \nabla \mathbf{u}) d\Omega. \end{aligned} \quad (3)$$

Using Eq. (3) in Eq. (1) the following expression of the weak $\{\mathbf{u}, \mathbf{P}\}$ formulation is obtained

$$\begin{aligned}
& \int_{\Omega_p} [\tilde{\boldsymbol{\sigma}}^S(\mathbf{u}) : \boldsymbol{\varepsilon}^S(\delta\mathbf{u}) - \tilde{\rho}\omega^2\mathbf{u} \cdot \delta\mathbf{u}] d\Omega \\
& + \int_{\Omega_p} \left[\frac{h^2}{\omega^2\tilde{\rho}_{22}} \nabla P \cdot \nabla \delta P - \frac{h^2}{\tilde{R}} P \delta P \right] d\Omega \\
& - \left[\tilde{\gamma} + h \left(1 + \frac{\tilde{Q}}{\tilde{R}} \right) \right] \int_{\Omega_p} \delta(\nabla P \cdot \mathbf{u}) d\Omega \\
& - h \left(1 + \frac{\tilde{Q}}{\tilde{R}} \right) \int_{\Omega_p} \delta(P \nabla \cdot \mathbf{u}) d\Omega \\
& - \int_{\partial\Omega_p} [\tilde{\boldsymbol{\sigma}}^t(\mathbf{u}) \cdot \mathbf{n}] \cdot \delta\mathbf{u} - \int_{\partial\Omega_p} h(U_n - u_n) \delta P dS = 0. \quad (4)
\end{aligned}$$

The weak form of the mixed pressure-displacement formulation [Eq. (4)] presents two interesting features. First, the symmetric coupling terms between the two phases are expressed in terms of volume integrals over the domain Ω_p . Second, the boundary integral terms involve the total stress tensor and the displacement flux at the boundary of the domain. Therefore, the application of coupling conditions with another domain, as well as boundary conditions and excitations, is achieved in a simpler manner compared to Eq. (1).¹²

B. Hierarchical elements

In the following, the approximation of Eq. (4) using 8-nodes parallelipipedic volume hierarchical elements is considered. The so-called ‘‘blending function method’’ is generally used to map this parent element into the geometrical element.²² Any point of the discretized subdomain with global coordinates (x, y, z) is located on a parent element by a set of local coordinates (ξ, η, ζ) . The relation between local and global coordinates is given by

$$\begin{pmatrix} x \\ y \\ z \end{pmatrix} = \sum_{i=1}^8 \begin{pmatrix} X_i \\ Y_i \\ Z_i \end{pmatrix} \cdot \mathcal{N}_i(\xi, \eta, \zeta) + \sum_{j=1}^{12} \begin{pmatrix} l_j^x \\ l_j^y \\ l_j^z \end{pmatrix} \cdot l_j^1 \cdot l_j^2. \quad (5)$$

In Eq. (5), $\langle X_i, Y_i, Z_i \rangle$ stands for the global coordinates of node i . The functions \mathcal{N}_i are the classic linear basis functions used in finite elements and are related to node i on the parent element. In order to consider complex geometries for an element, additional functions related to the edge j are taken into account. These functions correspond to the term on the right-hand side of Eq. (5). l_j^1 and l_j^2 are linear functions depending on a single local coordinate (different for l_j^1 and l_j^2) ξ , η , or ζ . l_j^x , l_j^y , and l_j^z are functions depending on the third local coordinate and used for the description of edge j . Further details are given in Ref. 22.

The next step is the interpolation of the fields on the mesh provided for the subdomain. On a given element, the variable q is approximated by

$$q(\xi, \eta, \zeta) = \sum_i \mathcal{N}_i(\xi, \eta, \zeta) q_i^{\text{ph}} + \sum_j \mathcal{G}_j(\xi, \eta, \zeta) q_j^{\text{gen}}. \quad (6)$$

In Eq. (6), \mathcal{N}_i are called node modes and are identical to those used in Eq. (5). The associated amplitudes q_i^{ph} stand for the physical value of q at node i (the superscript ph means physical). Functions \mathcal{G}_j are additional shape functions classified in three categories: edge modes, face modes, and internal modes. The associated generalized amplitudes q_j^{gen} (the superscript gen means generalized) do not have simple physical meaning. Like node modes, edge and face modes are associated to a geometrical entity of the mesh. For example, an edge mode on an element is associated with a particular edge j of this element. Its value is 0 on all the other edges of the element. As for internal modes, their value is 0 on all the faces of the element. By considering each category of modes explicitly, Eq. (6) rewrites

$$\begin{aligned}
q(\xi, \eta, \zeta) &= \sum_i \mathcal{N}_i(\xi, \eta, \zeta) q_i^{\text{ph}} + \sum_j \mathcal{E}_j(\xi, \eta, \zeta) q_j^{\text{gen}} \\
&+ \sum_k \mathcal{F}_k(\xi, \eta, \zeta) q_k^{\text{gen}} + \sum_l \mathcal{I}_l(\xi, \eta, \zeta) q_l^{\text{gen}}, \quad (7)
\end{aligned}$$

where \mathcal{E}_j are edge modes, \mathcal{F}_k are face modes, and \mathcal{I}_l are internal modes. These functions are chosen to make complete polynomials of ascending order p . Namely, the basis functions of the hierarchical variables are constructed using Legendre polynomials. The number of basis functions depends on the interpolation order p . The selection process, detailed in Ref. 22, leads to the expression of the generalized shape functions; they are given in the Appendix for completeness. Note that the present approach considers a mapping of the parent element into the geometrical element, using only the functions \mathcal{N}_i in Eq. (5).

C. Numerical implementation

As previously stated, in the present approach, the weak integral formulation given by Eq. (4) is discretized using 8-node volume elements. The displacement of the solid phase \mathbf{u} and the pressure in the pores P are expanded in terms of node modes and hierarchical shape functions. Hence, the field variables in a given element are written in the following form:

$$\mathbf{u}^e = [N_s] \{u_n\}^e \quad \text{and} \quad p^e = [N_f] \{p_n\}^e, \quad (8)$$

where $[N_s]$ and $[N_f]$ are the interpolation matrices on the considered element e . $\{u_n\}^e$ and $\{p_n\}^e$ stand for the physical and generalized amplitudes associated with the displacement of the solid phase and the pressure in the pores, respectively.

1. Discretization of the weak form

Substituting Eq. (8) into Eq. (4), one gets

$$\int_{\Omega_p} \tilde{\boldsymbol{\sigma}}^S(\mathbf{u}) : \boldsymbol{\varepsilon}^S(\delta\mathbf{u}) d\Omega \Rightarrow \langle \delta u_n \rangle [K] \{u_n\}, \quad (9)$$

$$\int_{\Omega_p} \tilde{\rho}\omega^2 \mathbf{u} \cdot \delta\mathbf{u} d\Omega \Rightarrow \langle \delta u_n \rangle [\tilde{M}] \{u_n\}, \quad (10)$$

$$\left[\tilde{\gamma} + h \left(1 + \frac{\tilde{Q}}{\tilde{R}} \right) \right] \int_{\Omega_p} \delta \mathbf{u} \cdot \nabla P \, d\Omega \Rightarrow \langle \delta u_n \rangle [\tilde{C}_1] \{P_n\}, \quad (11)$$

$$h \left(1 + \frac{\tilde{Q}}{\tilde{R}} \right) \int_{\Omega_p} P \nabla \cdot \delta \mathbf{u} \, d\Omega \Rightarrow \langle \delta u_n \rangle [\tilde{C}_2] \{P_n\}, \quad (12)$$

$$\frac{h^2}{\tilde{\rho}_{22}} \int_{\Omega_p} \nabla P \cdot \nabla \delta P \, d\Omega \Rightarrow \langle \delta P_n \rangle [\tilde{H}] \{P_n\}, \quad (13)$$

$$\frac{h^2}{\tilde{R}} \int_{\Omega_p} P \delta P \, d\Omega \Rightarrow \langle \delta P_n \rangle [\tilde{Q}] \{P_n\}, \quad (14)$$

where $\{u_n\}$ and $\{P_n\}$ represent the solid and fluid phase physical and generalized degrees of freedom of the whole mesh. $[K]$ and $[\tilde{M}]$ are, respectively, the stiffness and mass matrix associated to the solid phase *in vacuo*. $[\tilde{H}]$ and $[\tilde{Q}]$ are, respectively, the kinetic and compressional energy matrices of the fluid phase. $[\tilde{C}_1]$ and $[\tilde{C}_2]$ stand for the coupling between the two phases of the porous medium. The notation $[\tilde{\cdot}]$ indicates that the matrices are complex valued and frequency dependent. Note that compared to the implementation of the $\{\mathbf{u}, \mathbf{P}\}$ formulation presented in Ref. 11, two new matrices have to be computed. In the theory of hierarchical elements, the basis functions on an element are built using Legendre polynomials. The computation of the matrices in Eqs. (9)–(14) is performed with the commonly used Gauss–Legendre integration scheme and enough integration points are chosen to ensure a correct approximation. This step is time consuming and is the main drawback of hierarchical elements.²⁴ To alleviate that problem, Hinnant²⁵ proposed the “vector quadrature” integration scheme. However, this optimization procedure is not used in the present approach.

Substituting Eqs. (9)–(14) in the weak formulation leads to the following system to be solved:

$$\begin{pmatrix} [K] - \omega^2 [\tilde{M}] & -[\tilde{C}_1] - [\tilde{C}_2] \\ -\omega^2 [\tilde{C}_1]^T - \omega^2 [\tilde{C}_2]^T & [\tilde{H}] - \omega^2 [\tilde{Q}] \end{pmatrix} \begin{Bmatrix} u_n \\ P_n \end{Bmatrix} = \begin{Bmatrix} F_s \\ F_p \end{Bmatrix}, \quad (15)$$

where the right-hand side of the equation denotes the loading vector for the porous material. The application of various loading conditions is described in the following paragraph. The coupled system given by Eq. (15) is similar to the one obtained in classical finite elements.

2. Application of boundary and loading conditions

The boundary conditions and the loading terms involved in the $\{\mathbf{u}, \mathbf{P}\}$ formulation were presented by Debergue *et al.*¹² Their application in the context of the theory of hierarchical elements is detailed hereafter. In the present paper, three boundary conditions are considered. The porous material can be (i) bonded onto a rigid wall, (ii) guided, or (iii) free (i.e., not subject to any boundary condition). In case (i), the displacement vector of the solid phase is set to 0. In case (ii), the normal component to the interface of the solid phase displacement is set to 0. In case (iii), the fluid pressure is set

to 0 on the interface (note that this condition is approximate and its accuracy is discussed by Debergue¹²). Therefore, for an element on the boundary, applying the boundary conditions mentioned above amounts to setting to 0 one or several components of the fields. This is achieved by constraining the amplitudes of the modes of the nodes, edges and faces lying on the boundary and related to the considered component of the fields. Practically, the coefficients of the matrices in Eqs. (9)–(14) relative to these degrees of freedom are not assembled. Note that, by construction, the value of internal modes are worth 0 on each face of the element and thus are not subject to the above mentioned conditions. In the configurations studied in this paper, two kinds of loads have been considered. First, the load is a rigid piston motion imposed on one side of the porous material. This leads to the following condition on the interface:

$$\mathbf{u} \cdot \mathbf{n} = u_0, \quad (u_n - U_n) = 0, \quad (16)$$

where \mathbf{n} is the normal to the interface, and u_0 the amplitude of the piston motion. Second, the porous medium is submitted to an acoustical excitation, which can be modeled as an imposed surface pressure of amplitude p_0 . The condition at the interface is then

$$p = p_0, \quad \tilde{\sigma}^t \cdot \mathbf{n} = -p_0 \mathbf{n}. \quad (17)$$

To be concise, the two considered kinds of excitations lead to an imposed value q_0 of a component q of the fields in the porous material. Considering the expression of q given by Eq. (6) the following conditions must be imposed on the interface:

$$\{q^{\text{ph}}\} = \{q_0\} \quad \text{and} \quad \{q^{\text{gen}}\} = 0. \quad (18)$$

Equation (18) means that the values of q have to be set to q_0 at the nodes on the interface. Besides, the amplitudes of the hierarchical shape functions related to the edges or faces located on the interface are set to 0. By definition, the amplitudes of the internal modes are null on the sides of an element. The conditions of imposed degrees of freedom expressed by Eq. (18) are taken into account in the discretized weak formulation using discrete Lagrange multipliers.

In addition, when a surface pressure with amplitude p_0 is imposed, Eq. (17) leads to an elementary force vector given by

$$\{F_s\}_{\text{elem}} = - \int_{\partial \Omega_{p \text{ elem}}} p_0 \mathbf{n} \cdot [N_s] \, dS, \quad (19)$$

where $[N_s]$ is the column vector containing the shape function related to the face if the considered element subject to the excitation. Note that only node modes, edge modes with interpolation order $p=2$, and face modes with interpolation order $p=4$ are taken into account in $[N_s]$. In fact, the other modes of analytical expression \mathcal{G} verify the following relation by construction:

$$\int_{\partial \Omega_{p \text{ elem}}} \mathcal{G} \, dS = 0. \quad (20)$$

The proof for this assertion is given in the Appendix. Note that for all the excitations considered in this paper, $\{F_p\} = 0$ in Eq. (15).

3. Vibroacoustics indicators

In the result section, two vibroacoustic indicators are considered. For the solid phase of the porous material, the mean square velocity along the three directions is computed. Practically, the mean square velocity along direction i is given by

$$\begin{aligned} \langle v_i^2 \rangle &= \frac{\omega^2}{2\Omega_p} \int_{\Omega_p} |v_i|^2 d\Omega \\ &= \frac{\omega^2}{2\Omega_p} \langle u_n^{\text{ph}} \ u_n^{\text{gen}} \rangle^* [M_i] \left\{ \begin{matrix} u_n^{\text{ph}} \\ u_n^{\text{gen}} \end{matrix} \right\}, \end{aligned} \quad (21)$$

where $\langle u_n^{\text{ph}} \ u_n^{\text{gen}} \rangle$ is the row vector containing the physical and generalized amplitudes relative to the solid phase displacement along direction i . $[M_i]$ contains the coefficients of a partition of the mass matrix $[\tilde{M}]$ divided by $\tilde{\rho}$ and related to the appropriate degrees of freedom. In Eq. (21), $(*)$ means complex conjugate, and Ω_p is the volume of the poroelastic domain.

For the fluid phase, the mean square pressure is computed using the following formula:

$$\begin{aligned} \langle P^2 \rangle &= \frac{1}{2\Omega_p} \int_{\Omega_p} |P|^2 d\Omega \\ &= \frac{1}{2\Omega_p} \langle P_n^{\text{ph}} \ P_n^{\text{gen}} \rangle^* [Q_1] \left\{ \begin{matrix} P_n^{\text{ph}} \\ P_n^{\text{gen}} \end{matrix} \right\}, \end{aligned} \quad (22)$$

where $\langle P_n^{\text{ph}} \ P_n^{\text{gen}} \rangle$ is the row vector of the physical and generalized amplitudes related to the pressure in the pores. $[Q_1]$ is the compression matrix of the fluid phase $[\tilde{Q}]$ divided by h^2/\bar{R} .

III. NUMERICAL EXAMPLES

In the following, the validation of the $\{u, P\}$ formulation using hierarchical elements is numerically assessed. The present approach is compared to a finite element code developed at the Université de Sherbrooke and based on classical finite elements. This latter code has been validated both numerically and experimentally, elsewhere.^{11,12} The accuracy of the results obtained by the use of hierarchical elements is underlined. The reduction of the number of degrees of freedom provided by the use of high order polynomials for the basis functions is highlighted, thus illustrating the performances of hierarchical poroelastic elements. An emphasis is made on this latter aspect by showing the benefit of using different interpolation orders for the basis functions of each phase. Finally, the convergence of the hierarchical poroelastic elements is investigated in the case of a particular material with several boundary conditions and excitations.

The studied problem consists of a single porous material with a rear face bonded onto a rigid wall (see Fig. 1). The boundary conditions on the lateral faces are either (i) free, or (ii) bonded. Two kinds of loads are used in the following, depending on the boundary conditions on the edges of the porous medium. In case (i), the porous medium is subjected to a rigid piston motion with a 10^{-3} m amplitude normal displacement [hereby referred to as configuration (i)]. In case (ii) a surface pressure of amplitude 1 Pa is imposed on the

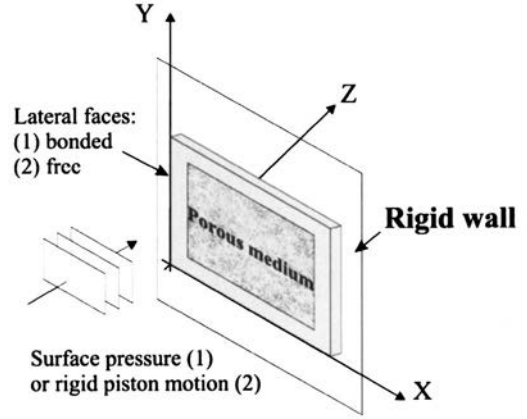


FIG. 1. Configuration of the problem.

front face [hereby referred to as configuration (ii)]. A 5 cm thick porous material with lateral dimensions $0.35 \text{ m} \times 0.22 \text{ m}$ is considered. Among the vibroacoustic indicators presented in the preceding section, only the mean square velocity along z axis (denoted $\langle V_z^2 \rangle$) and the mean quadratic pressure (denoted $\langle P^2 \rangle$) are studied. Actually the mean quadratic velocities along the lateral dimensions of the porous material are of limited interest in vibroacoustic applications.

A. Validation

In this subsection, the accuracy and the performance of the present approach is numerically assessed. In the following, the results obtained with hierarchical elements and finite elements are compared to a reference value. In the present paper, this reference is obtained by increasing considerably the interpolation orders for a fixed mesh when hierarchical elements are used, in order to be sure that convergence is reached. The same results can be obtained with classical finite elements but require a very refined mesh and thus huge computational resources. Hence, the classical finite element implementation has not been used for obtaining the reference values. In the following, the interpolation orders for the basis functions given a fixed mesh for the present approach or the classical finite element mesh are said to be acceptable when the response of the porous material is predicted within a tolerance from the reference response. This tolerance is fixed to 0.5 dB from the reference curve and 5% in the location of resonance peaks.

The first validation test consists in configuration (i). The material studied is a wool, UGW3, with characteristics given in Table I. $\langle P^2 \rangle$ is computed as a function of frequency and is actually the indicator which proves to have the most difficulties to converge. The results obtained with the classical code and the present approach with different meshes are presented in Fig. 2. Note that the maximum difference between the different meshes, including classical finite elements, and the reference curve is less than 0.5 dB which is within the defined convergence criterion. For the modeling with hierarchical elements, parameters for the mesh, namely the number of elements and the order of the basis functions, are given in the following form $n_x * n_y * n_z$ elements $(p_s - p_f)$ where n_x , n_y , n_z denote the number of elements used in directions x , y , z , respectively, and p_s , p_f denote the interpolation order of

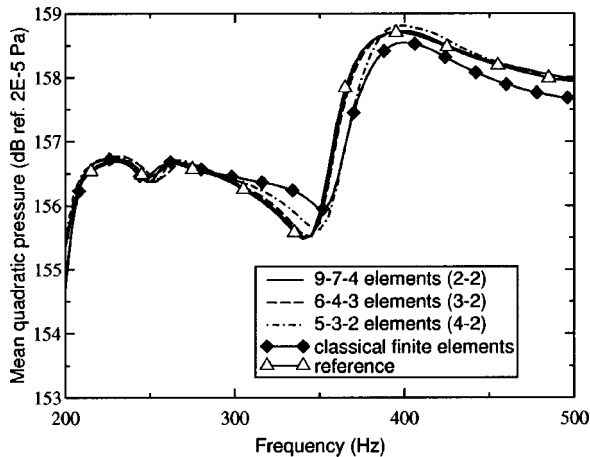
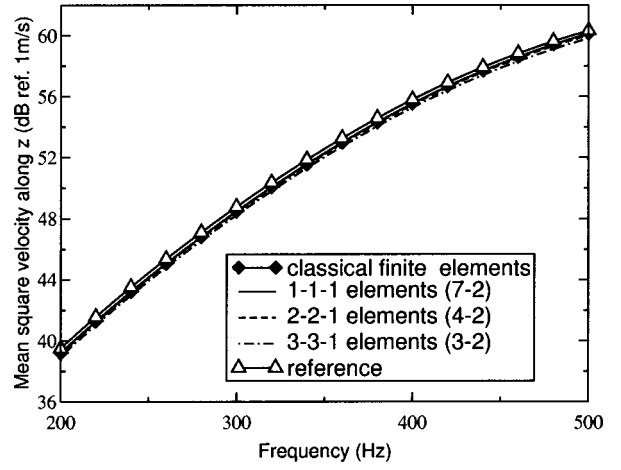
TABLE I. Characteristics of the materials.

Material	h	σ kN s/m ⁴	α_∞	Λ μm	Λ' μm	ρ_S kg/m ³	N kPa	ν	η
FM2	0.9	25	7.8	226	226	300	286	0.4	0.265
UGW3	0.95	25	1.4	93.2	93.2	600	21	0	0.05

the basis functions for the solid phase and the fluid phase, respectively. Figure 2 shows that the present approach leads to accurate results for all tested meshes. To test the ability of the hierarchical poroelastic element to model different materials in various configurations a foam, FM2, with characteristics given in Table I is considered in configuration (ii). $\langle V_z^2 \rangle$ is computed as a function of frequency; this indicator has the most difficulties to converge. The results are presented in Fig. 3. Once again, accurate results are obtained with the hierarchical poroelastic elements for different meshes.

The excellent results for the two previous validation tests show the validity of the present approach. In addition, hierarchical poroelastic elements prove to be very performant. Tables II and III summarize the number of degrees of freedom (dof) required to ensure convergence, either with classical finite elements or hierarchical elements. Each of the two configurations studied above are considered. For the present approach, the number of degrees of freedom is given for different meshes and the corresponding required interpolation orders. Actually, the present approach allows for an important decrease of the number of dof required to satisfy the convergence criterion defined previously (0.5 dB from the reference curve and 5% accuracy in the location of resonance peaks). Moreover, the best performance is achieved using a coarse mesh and a high interpolation order for the basis functions. This trend has already been pointed out for the modeling of elastic materials using hierarchical elements in static problems.²²

As seen in Tables II and III, the interpolation order for the basis functions can be chosen to be different for the two phases of the porous material. Actually, the solid and the fluid phase exhibit different physical behaviors depending on the studied configuration. This feature of the hierarchical poroelastic elements is of great interest since convergence is ensured by choosing the adequate interpolation order for


 FIG. 2. $\langle P^2 \rangle$ for glasswool UGW3 in configuration (i).

 FIG. 3. $\langle V_z^2 \rangle$ for a foam FM2 in configuration (ii).

each phase separately. On the other hand, convergence in classical finite elements is ensured by refining the mesh, i.e., a refined description of both phases of the porous material. Hence, the former approach provides an efficient way for the reduction of the number of degrees of freedom required for a correct modeling of the material.

B. Convergence of the vibroacoustic indicators

In the following, foam FM2 is studied in configurations (i) and (ii). The geometry of the porous sample is identical to the one considered previously. The frequency range of interest is [0 Hz; 500 Hz]. Biot's theory of poroelasticity² indicates that two compression waves (denoted P_1 and P_2 in the following) and a shear wave (denoted S) can propagate simultaneously in a porous medium. For each kind of wave, the ratio μ of the fluid phase displacement to the solid phase displacement can be computed.³ These ratio at 500 Hz for foam FM2 are given in Table IV. Table IV indicates that waves P_1 and S propagate in both phases. On the contrary, wave P_2 propagates mainly in the fluid phase, so that the two phases of the porous material can be considered as decoupled as far as wave P_2 is concerned. This point strongly influences the behavior of the porous materials according to the configuration studied. Foam FM2 has been previously studied in configuration (ii). Excellent values for $\langle V_z^2 \rangle$, represented in Fig. 3, can be obtained with low interpolation order for the basis functions of the fluid phase. This means that a coarse description of the fluid phase suffices for the convergence of this indicator related to the solid phase. Indeed, this porous material in configuration (ii) is subjected to an acoustical excitation acting on both phases. The pressure in the pores and the stress tensor in the solid phase *in vacuo* are imposed at the interface where the material is excited. Because wave P_2 mainly propagates in the fluid phase, the fluid phase has a weak influence on the solid phase and thus does

 TABLE II. Convergence of $\langle V_z^2 \rangle$ for FM2 in configuration (ii).

Nb of elements		1-1-1	2-2-1	3-3-1
interpolation order (solid-fluid)	Classical code	7-2	4-2	3-2
Number of dof	2144	70	144	244

TABLE III. Convergence of $\langle P^2 \rangle$ for UGW3 in configuration (i).

Nb of elements		4-3-2	5-3-2	6-4-3	9-7-4
interpolation order (solid-fluid)	Classical code	3-2	3-2	3-2	2-2
Number of dof	5214	895	1094	2397	4828

not require a very accurate description for the convergence of $\langle V_z^2 \rangle$: the motion in the solid phase is due to wave P_1 and S . In comparison, indicator $\langle P^2 \rangle$ for foam FM2 in the same configuration is represented in Fig. 4. Different interpolation orders have been used with a fixed $2 \times 2 \times 1$ elements mesh for the present approach. Compared to $\langle V_z^2 \rangle$, $\langle P^2 \rangle$ requires a noticeable lower interpolation order for the basis functions in the solid phase. This indicates that a coarse representation of the solid phase suffices for the convergence of this latter indicator. The influence of waves P_1 and S on the motion of the fluid phase is not significant. Actually the motion of the fluid phase is mainly due to wave P_2 .

Next, consider foam FM2 in configuration (i). As previously, $\langle P^2 \rangle$ is plotted as a function of frequency in Fig. 5. It can be observed that a higher interpolation order for the basis functions of the solid phase in comparison with configuration (ii) is required for the convergence of $\langle P^2 \rangle$. In this configuration, the porous is submitted to a rigid piston motion. For that kind of excitation, the solid phase is directly excited and its motion is strongly transmitted to the fluid when the amplitude ratios μ are important for waves P_1 and S . Hence, in configuration (i) the motion of the fluid phase is mainly due to these latter waves. In conclusion, the two phases of a porous material can exhibit very different behaviors according to the excitation. This induces a convergence which highly depends on the configuration studied for the considered vibroacoustic indicators, namely $\langle V_z^2 \rangle$ or $\langle P^2 \rangle$. Hence, it is difficult to conclude about the convergence of a set of indicators in a general manner.

C. Investigation of the convergence of hierarchical poroelastic elements

For 3D deformations, the classical convergence criterion gives indications for a minimal mesh but is insufficient because of locking of 3D linear elements and discrepancies of the fields in the two phases of the porous material. As stated in Sec. III A, the use of the theory of hierarchical elements together with the $\{\mathbf{u}, \mathbf{P}\}$ formulation enables one to solve these latter problems and to get smaller linear systems to solve.

In this section, the convergence of hierarchical poroelastic elements is investigated for a particular material, wool UGW3. The aim of this study is to determine the interpolation order for the basis functions in the two phases of the porous material that allows for convergence given the element size. Initially, the motivation for this study was to de-

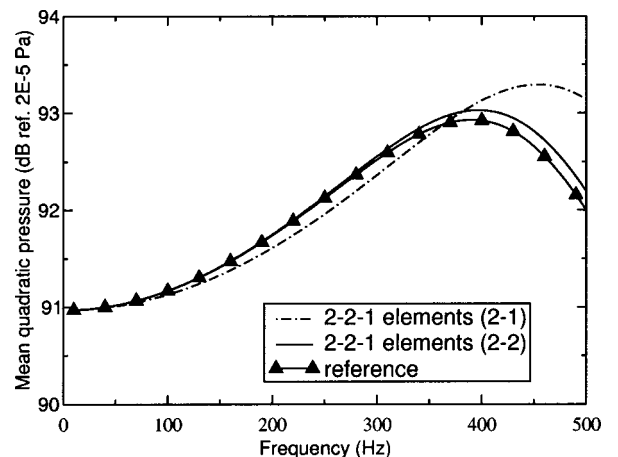
TABLE IV. Amplitude ratios for foam FM2 at 500 Hz.

Kind of wave	P_1	P_2	S
Amplitude ratio μ	$0.998 + 0.161 \times i$	$-10.43 + 1.70 \times i$	$0.97 - 1.14 \times i$

rive a convergence criterion that could be reused for other porous materials. However, it appears that the results for wool UGW3 cannot be directly transposed and that only a convergence study performed on different materials would enable one to draw general trends for the convergence of hierarchical poroelastic elements. This task implies a huge amount of calculations. Therefore, only preliminary results are given here. This convergence study is however helpful to highlight the influence of the coupling between the two phases of wool UGW3 as it is shown thereafter and to confirm the observations made on foam FM2 in Sec. III B.

In the following, the mesh in the lateral dimensions of a 3D porous sample is studied. As a consequence, the number of elements along the thickness is chosen large enough so that only the lateral mesh influences the results. For a chosen indicator, the interpolation order in both phases can be represented as a function of the element size. In order to have nondimensional data in the abscissa, the element size is scaled to the wavelength λ of wave P_1 , P_2 or S at the highest frequency in the frequency range of interest. These wavelengths at 500 Hz are given in Table V. As these wavelengths are rather short, a wide range of element size to wavelength ratio is provided. The study that follows is carried out for each of the two configurations (i) and (ii) depicted in Sec. III A and for each vibroacoustic indicator ($\langle V_z^2 \rangle$ and P^2) according to remarks in Sec. III B.

Configuration (i): The interpolation orders for the solid phase (respectively, fluid phase) basis functions that ensure the convergence of the two indicators $\langle P^2 \rangle$ and $\langle V_z^2 \rangle$ are plotted as a function of the ratio of the element size to λ_{P_1} , where λ_{P_1} denotes the wavelength of wave P_1 at 500 Hz. The results are represented in Fig. 6 (respectively, Fig. 7). In these figures, fit curves are provided for clarity. Note that the wavelength of another kind of wave, e.g., S wave or P_2 , can be chosen to scale the element size simply by multiplying the


 FIG. 4. $\langle P^2 \rangle$ for foam FM2 in configuration (ii).

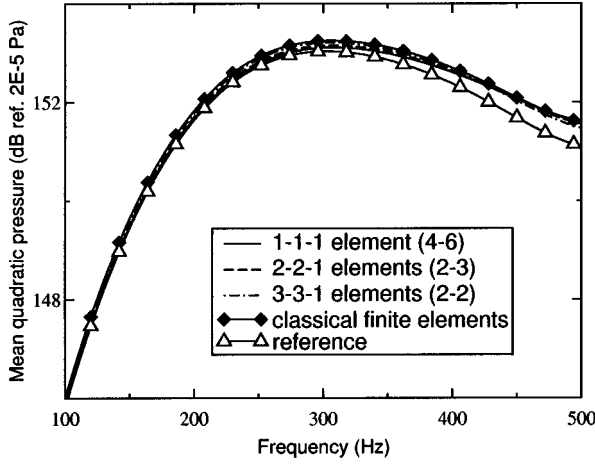


FIG. 5. $\langle P^2 \rangle$ for foam FM2 in configuration (i).

abscissa in Figs. 6 and 7 by the factor λ_{P_1}/λ_S or $\lambda_{P_1}/\lambda_{P_2}$.

Considering a fixed mesh, it is seen in Figs. 6 and 7 that the convergence of indicator $\langle P^2 \rangle$ is not solely governed by the interpolation order for the basis functions in the fluid phase. Indeed, a sufficiently high interpolation order for the basis functions in the solid phase is required to ensure the convergence of $\langle P^2 \rangle$. This interpolation is even higher than the one needed for the convergence of $\langle V_z^2 \rangle$. The opposite is observed regarding the interpolation order for the basis functions in fluid phase. This is because of important coupling phenomena between the two phases when the solid phase of the porous material is directly excited.

Configuration (ii): Like in configuration (i), the interpolation orders required for the convergence of the two indicators $\langle P^2 \rangle$ and $\langle V_z^2 \rangle$ are plotted as a function of the ratio of the element size to λ_{P_1} . These interpolation orders for the solid and the fluid phase are represented in Figs. 8 and 9, respectively. As previously, fit curves are provided for clarity. When considering the basis functions in the solid phase, Fig. 8 shows that for a fixed element size to λ_{P_1} , the interpolation order required for the convergence of $\langle P^2 \rangle$ is as high as the one for $\langle V_z^2 \rangle$, except for low size element to wavelength ratio. For the basis functions of the fluid phase, the interpolation order ensuring the convergence of $\langle V_z^2 \rangle$ is smaller than the one ensuring the convergence of $\langle P^2 \rangle$. Hence, from these observations, coupling phenomena between the two phases of the porous material appear to influence weakly the response of the porous material. This latter phenomenon can be explained by the fact that the porous material has bonded edges and is submitted to an acoustical excitation. To sum up the results found in this particular configuration, given a fixed mesh, the interpolation orders for the basis functions in the two phases of the porous material chosen to ensure simultaneously the convergence of $\langle P^2 \rangle$ and $\langle V_z^2 \rangle$ exhibit the following feature: regarding the basis

TABLE V. Wave numbers for the different kinds of waves in wool UGW3 at 500 Hz.

Kind of wave	P_1	P_2	S
Wavelength (m)	7.237×10^{-2}	1.962×10^{-1}	5.199×10^{-2}

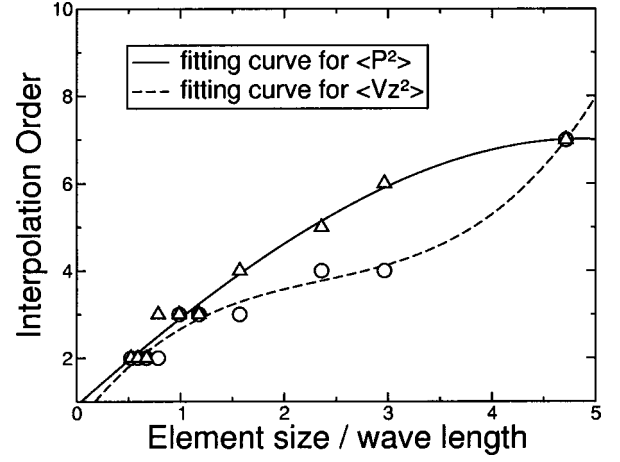


FIG. 6. Convergence criterion for the solid phase. Configuration (i). Given an element size for the mesh, an interpolation order in the solid phase that suffices for the convergence of $\langle P^2 \rangle$ (respectively, $\langle V_z^2 \rangle$) is determined by numerical experiments. Δ (respectively, \circ) stands for the corresponding couple of values interpolation order-element size to wavelength ratio.

functions in the solid phase (respectively, fluid phase), the choice of the interpolation order ensuring the convergence of $\langle V_z^2 \rangle$ (respectively, $\langle P^2 \rangle$) allows for the convergence of both indicators.

IV. CONCLUSION

The implementation of the $\{\mathbf{u}, \mathbf{P}\}$ formulation for porous materials using the theory of hierarchical elements has been presented. The use of high order polynomials for the basis functions enables one to solve some of the problems met with linear poroelastic elements, among them numerical locking and the presence of two different scale phenomena. Hence, hierarchical poroelastic elements allow for the prediction of the forced response of a porous material using a reduced number of degrees of freedom. The reduction of the number of unknowns is all the more effective than a coarse mesh with high interpolation orders is provided. Besides, the

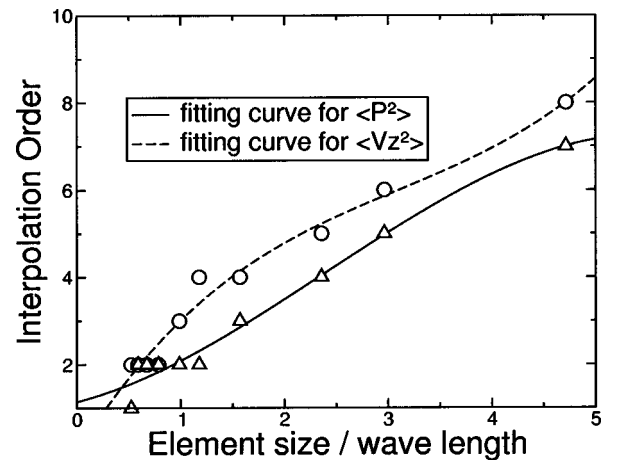


FIG. 7. Convergence criterion for the fluid phase. Configuration (i). Given an element size for the mesh, an interpolation order in the fluid phase that suffices for the convergence of $\langle P^2 \rangle$ (respectively, $\langle V_z^2 \rangle$) is determined by numerical experiments. Δ (respectively, \circ) stands for the corresponding couple of values interpolation order-element size to wavelength ratio.

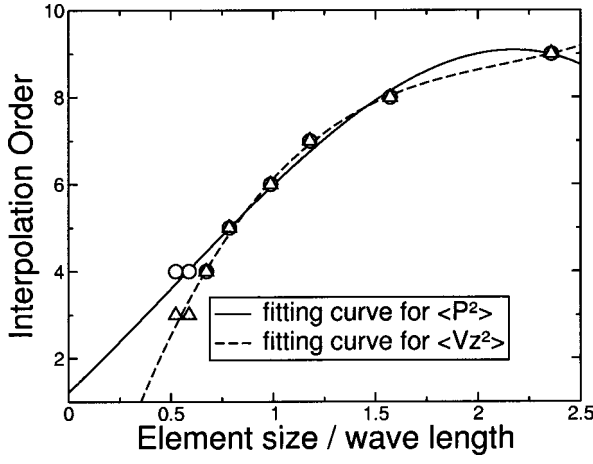


FIG. 8. Convergence criterion for the solid phase. Configuration (ii). Given an element size for the mesh, an interpolation order in the solid phase that suffices for the convergence of $\langle P^2 \rangle$ (respectively, $\langle V_z^2 \rangle$) is determined by numerical experiments. \circ (respectively, \triangle) stands for the corresponding couple of values interpolation order-element size to wavelength ratio.

performance of hierarchical elements is enhanced by the use of different interpolation orders for the basis functions of each phase separately.

Considering a particular material, a preliminary study has been conducted in order to link the interpolation order of the basis functions in the two phases of the porous material to the ratio of the element size to the wavelength. It has been found that for a mechanical excitation, each phase happens to influence strongly the vibratory state of the other phase, showing the importance of the coupling between the two phases of the porous material. Regarding interpolation order for the basis functions in the solid phase, this implies, for example, to chose an interpolation order for the convergence of $\langle P^2 \rangle$ larger than the one for $\langle V_z^2 \rangle$. This interaction phenomenon proves to be of least importance for an acoustical excitation. In this case, considering the basis functions in the solid phase, the interpolation order for the convergence of $\langle V_z^2 \rangle$ is found to be as large as for $\langle P^2 \rangle$. To derive more

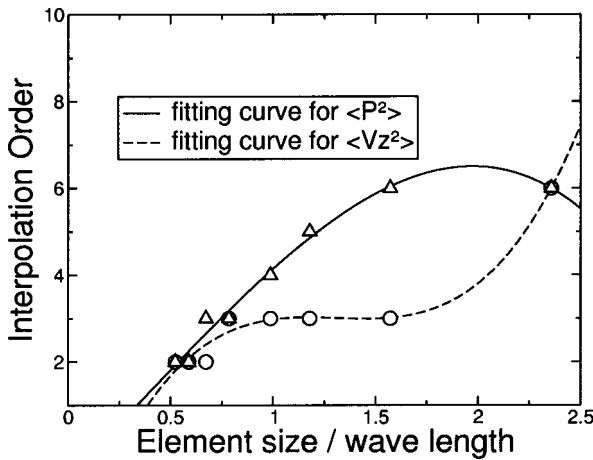


FIG. 9. Convergence criterion for the fluid phase. Configuration (ii). Given an element size for the mesh, an interpolation order in the fluid phase that suffices for the convergence of $\langle P^2 \rangle$ (respectively, $\langle V_z^2 \rangle$) is determined by numerical experiments. \triangle (respectively, \circ) stands for the corresponding couple of values interpolation order-element size to wavelength ratio.

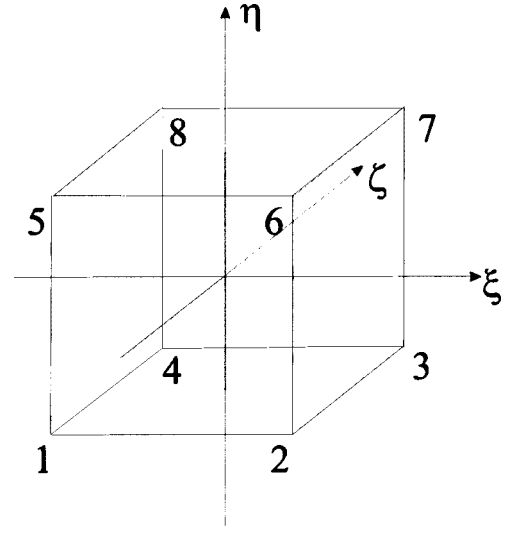


FIG. 10. The reference element and the standard numbering of nodes.

general trends for the convergence of hierarchical poroelastic elements, further works involving the study of other kinds of materials are required. However, the presented examples show the difficulty of deriving a general meshing criterion for porous-elastic materials. More importantly, they highlight the importance of conducting a serious convergence study before any vibroacoustic study regarding the behavior of porous-elastic materials, based on using finite element codes.

APPENDIX

The shape functions involved in the approximation of the fields on one element [Eq. (6)] are defined on a parent element, which is an 8-noded brick element represented in Fig. 10. On that element, the geometrical entities (nodes, edges, and faces) are assigned a number. From this follows the definition of the basis shape functions.

1. Node modes

A node mode of analytical expression \mathcal{N}_i , is related to node i on the parent element. \mathcal{N}_i is a linear function of the local coordinates and has value 1 at node i and 0 at the other nodes. Node modes are given by

$$\mathcal{N}_1(\xi, \eta, \zeta) = \frac{1}{8}(1 - \xi)(1 - \eta)(1 - \zeta),$$

$$\mathcal{N}_2(\xi, \eta, \zeta) = \frac{1}{8}(1 + \xi)(1 - \eta)(1 - \zeta),$$

$$\mathcal{N}_3(\xi, \eta, \zeta) = \frac{1}{8}(1 + \xi)(1 + \eta)(1 - \zeta),$$

$$\mathcal{N}_4(\xi, \eta, \zeta) = \frac{1}{8}(1 - \xi)(1 + \eta)(1 - \zeta),$$

$$\mathcal{N}_5(\xi, \eta, \zeta) = \frac{1}{8}(1 - \xi)(1 - \eta)(1 + \zeta),$$

$$\mathcal{N}_6(\xi, \eta, \zeta) = \frac{1}{8}(1 + \xi)(1 - \eta)(1 + \zeta),$$

$$\mathcal{N}_7(\xi, \eta, \zeta) = \frac{1}{8}(1 + \xi)(1 + \eta)(1 + \zeta),$$

$$\mathcal{N}_8(\xi, \eta, \zeta) = \frac{1}{8}(1 - \xi)(1 + \eta)(1 + \zeta).$$

2. Edge modes

The edge i linking two nodes of the parent element is associated one or several edge modes. One particular edge

mode of analytical expression \mathcal{E}_p has zero value on all the edges of the parent element except on edge j . On this particular edge, its expression is a polynomial with order p . The general expression of the edges modes for $p \geq 2$ are given by

$$\begin{aligned}\mathcal{E}_p^{12} &= \frac{1}{4}\phi_p(\xi)(1-\eta)(1-\zeta), \\ \mathcal{E}_p^{23} &= \frac{1}{4}\phi_p(\eta)(1+\xi)(1-\zeta), \\ \mathcal{E}_p^{34} &= \frac{1}{4}\phi_p(\xi)(1+\eta)(1-\zeta), \\ \mathcal{E}_p^{41} &= \frac{1}{4}\phi_p(\eta)(1-\xi)(1-\zeta), \\ \mathcal{E}_p^{15} &= \frac{1}{4}\phi_p(\zeta)(1-\xi)(1-\eta), \\ \mathcal{E}_p^{26} &= \frac{1}{4}\phi_p(\zeta)(1+\xi)(1-\eta), \\ \mathcal{E}_p^{37} &= \frac{1}{4}\phi_p(\zeta)(1-\xi)(1+\eta), \\ \mathcal{E}_p^{48} &= \frac{1}{4}\phi_p(\zeta)(1+\xi)(1+\eta), \\ \mathcal{E}_p^{56} &= \frac{1}{4}\phi_p(\xi)(1-\eta)(1+\zeta), \\ \mathcal{E}_p^{67} &= \frac{1}{4}\phi_p(\eta)(1+\xi)(1+\zeta), \\ \mathcal{E}_p^{78} &= \frac{1}{4}\phi_p(\xi)(1+\eta)(1+\zeta), \\ \mathcal{E}_p^{85} &= \frac{1}{4}\phi_p(\eta)(1-\xi)(1+\zeta),\end{aligned}$$

where the superscript kl indicates that the considered edges is defined by node k and node l on the parent element. Functions ϕ_p are built using orthogonal Legendre polynomials L_p and are obtained by the formula

$$\phi_p(\xi) = \frac{1}{\sqrt{2(2j-1)}}(L_p(\xi) - L_{p-2}(\xi)) \quad \text{with } p \geq 2. \quad (\text{A1})$$

The relations verified by functions ϕ_p are given further on.

3. Face modes

Each face i of the parent element is associated with face modes which are zero on all the faces of the parent element except for face i . Considering the interpolation order $p \geq 4$, one or several couples of integers (k_1, k_2) verifying $k_1 + k_2 = p$ are constituted. Note that the couple (k_1, k_2) is different from the couple (k_2, k_1) . Each couple is associated a mode related to face i . The general expression for this mode $\mathcal{F}_{k_1 k_2}$ is given by

$$\begin{aligned}\mathcal{F}_{k_1 k_2}^{1265} &= \frac{1}{2}\phi_{k_1}(\xi)\phi_{k_2}(\zeta)(1-\eta), \\ \mathcal{F}_{k_1 k_2}^{2376} &= \frac{1}{2}\phi_{k_1}(\eta)\phi_{k_2}(\zeta)(1-\xi), \\ \mathcal{F}_{k_1 k_2}^{1234} &= \frac{1}{2}\phi_{k_1}(\xi)\phi_{k_2}(\eta)(1-\zeta), \\ \mathcal{F}_{k_1 k_2}^{4158} &= \frac{1}{2}\phi_{k_1}(\eta)\phi_{k_2}(\zeta)(1+\xi), \\ \mathcal{F}_{k_1 k_2}^{3487} &= \frac{1}{2}\phi_{k_1}(\xi)\phi_{k_2}(\zeta)(1+\eta), \\ \mathcal{F}_{k_1 k_2}^{5678} &= \frac{1}{2}\phi_{k_1}(\xi)\phi_{k_2}(\eta)(1+\zeta),\end{aligned}$$

where the superscript $klmn$ states for the face defined by the nodes k, l, m , and n .

4. Internal modes

For an interpolation order $p \geq 6$, sets of three integers (k_1, k_2, k_3) verifying $k_1 + k_2 + k_3 = p$ are considered. Note that the set (k_1, k_2, k_3) is different from the set (k_1, k_3, k_2) and (k_2, k_3, k_1) . Each set is associated with an internal mode of analytical expression $\mathcal{I}_{k_1 k_2 k_3}$ given by

$$\mathcal{I}_{k_1 k_2 k_3} = \phi_{k_1}(\xi) \cdot \phi_{k_2}(\eta) \cdot \phi_{k_3}(\zeta).$$

5. Features of functions ϕ_k

The functions ϕ_k introduced in the preceding sections satisfy some interesting properties. First, by construction,

$$\phi_k(-1) = \phi_k(1) = 0. \quad (\text{A2})$$

Also the first derivative of these functions are orthogonal, namely,

$$\int_{-1}^1 \phi'_m(\xi)\phi'_n(\xi)d\xi = \delta_{mn}. \quad (\text{A3})$$

Finally, let's consider the analytical expression of a particular edge mode with an interpolation order k , for example, \mathcal{E}_k^{12} . The integration of this mode on the parent element face pertaining to the nodes 1, 2, 3, 4 leads to

$$\int_{1234} \mathcal{E}_k^{12} dS = \int_{-1}^1 (1-\eta)d\eta \cdot \int_{-1}^1 \phi_k(\xi)d\xi. \quad (\text{A4})$$

For $k > 2$, the function ϕ_k verify the relation

$$\begin{aligned}\int_{-1}^1 \phi_k(\xi)d\xi &= \sqrt{\frac{2}{2j+1}} \left[\frac{1}{2k+1} [\phi_{k+1}(1) - \phi_{k+1}(-1)] \right. \\ &\quad \left. - \frac{1}{2k-3} [\phi_{k-1}(1) - \phi_{k-1}(-1)] \right]. \quad (\text{A5})\end{aligned}$$

Given Eq. (A2), the value of this integral is 0. Hence all the edge modes with an interpolation order $k > 2$ satisfy Eq. (20). The extension of this relation for the face modes with interpolation order $p > 4$ is straightforward.

¹M. Delany and E. Bazley, "Acoustic properties for fibrous absorbent materials," *Appl. Acoust.* **3**, 105 (1970).

²M. Biot, "The theory of propagation of elastic waves in a fluid-saturated porous," *J. Acoust. Soc. Am.* **28**, 168 (1956).

³J. Allard, *Propagation of Sound in Porous Media. Modeling Sound Absorbing Materials* (Elsevier, New York, 1993).

⁴J. Bolton and E. Green, "Normal incidence sound transmission through double panel," *Appl. Acoust.* **39**, 25 (1993).

⁵U. Ingard, *Notes on Sound Absorption Technology* (Noise Control Foundation, 1994).

⁶Y. Kang and J. Bolton, "Finite element modeling of isotropic porous materials coupled with acoustical finite elements," *J. Acoust. Soc. Am.* **98**, 635 (1995).

⁷Y. Kang and J. Bolton, "A finite element model for sound transmission through foam-lined double-panel structures," *J. Acoust. Soc. Am.* **99**, 2755 (1996).

⁸R. Panneton and N. Atalla, "Numerical prediction of sound transmission through finite multilayer systems with poroelastic materials," *J. Acoust. Soc. Am.* **100**, 346 (1996).

⁹R. Panneton and N. Atalla, "An efficient finite element scheme for solving the three-dimensional poroelasticity problem in acoustics," *J. Acoust. Soc. Am.* **101**, 3287 (1997).

¹⁰J. Coyette and H. Wynendaele, "A finite element model for predicting the acoustic transmission characteristics of layered structures," *INTERNOISE* 95 (1995), pp. 1279–1282.

- ¹¹N. Atalla, R. Panneton, and P. Debergue, "A mixed displacement-pressure formulation for poroelastic materials," J. Acoust. Soc. Am. **104**, 1444 (1998).
- ¹²P. Debergue, R. Panneton, and N. Atalla, "Boundary conditions for the weak formulation of the mixed (u,p) poroelasticity problem," J. Acoust. Soc. Am. **106**, 2383 (1999).
- ¹³N. Dauchez, S. Sahraoui, and N. Atalla, "Convergence of poroelastic finite elements based on biot displacement formulation," J. Acoust. Soc. Am. **109**, 33 (2001).
- ¹⁴P. Debergue, "Développement d'une formulation mixte déplacement-pression pour les matériaux poroélastiques (Development of a mixed displacement-pressure formulation for poroelastic materials)," Master thesis, University of Sherbrooke, 1997.
- ¹⁵F. Sgard, N. Atalla, and R. Panneton, "A modal reduction technique for the finite element formulation of biot's poroelasticity equations in acoustics," J. Acoust. Soc. Am. **102**, 3112 (1997).
- ¹⁶F. Sgard, N. Atalla, and R. Panneton, "A modal reduction technique for the finite element formulation of biot's poroelasticity equations in acoustics applied to multilayered structures," J. Acoust. Soc. Am. **103**, 2882 (1998).
- ¹⁷F. Sgard, N. Atalla, and R. Panneton, "A mixed wave-finite element approach for solving biot's poroelasticity equations in acoustics," J. Acoust. Soc. Am. **105**, 1195 (1999).
- ¹⁸N. Dauchez, S. Sahraoui, and N. Atalla, "Dissipation mechanisms in a porous layer bonded onto a plate," J. Sound Vib. (to be published).
- ¹⁹S. Rigobert, F. Sgard, and N. Atalla, "Investigation on the dissipative effects in a poroelastic plate," J. Acoust. Soc. Am. **105**, 1295 (1999).
- ²⁰I. Babuška and B. Szabò, "The p and hp version of the finite element method, basic principle and properties," SIAM Rev. **36**, 578 (1994).
- ²¹I. Babuška and B. Szabò, "On the rate of convergence of the finite element method," Int. J. Numer. Methods Eng. **18**, 323 (1982).
- ²²B. Szabò and I. Babuška, *Finite Element Analysis* (Wiley, New York, 1991).
- ²³B. Szabò, "Hierarchic plate and shell models based on p-extension," Analytical and Computational Models of Shells presented at the Winter Annual Meeting of ASME Computers and Engineering division (10–15 December 1982).
- ²⁴A. Côté, "Modélisation vibroacoustique dans le domaine des moyennes fréquences par éléments finis de type p (Modeling vibroacoustic problems in the medium frequency range using p elements)," Ph.D. thesis, University of Sherbrooke, 1998.
- ²⁵H. Hinnant, "Fast method of numerical quadrature for p-version finite element matrice," Int. J. Numer. Methods Eng. **37**, 3723 (1994).